Reconstructing the full modal structure of photonic states by stimulated-emission tomography in the low-gain regime

A. Keller,[1,2] A. Z. Khoury,[3] N. Fabre,[4] M. Amanti,[1] F. Baboux,[1] S. Ducci,[1] and P. Milman[1]
[1]*Laboratoire Matériaux et Phénomènes Quantiques, CNRS, Université Paris Cité, 75013 Paris, France*
[2]*Department de Physique, Université Paris-Saclay, 91405 Orsay Cedex, France*
[3]*Instituto de Física, Universidade Federal Fluminense, Niterói, Rio de Janeiro 24210-346, Brazil*
[4]*Departamento de Óptica, Facultad de Física, Universidad Complutense, 28040 Madrid, Spain*

(Received 18 May 2022; accepted 28 November 2022; published 14 December 2022)

Stimulated emission tomography (SET) is a powerful and successful technique to both improve the resolution and experimentally simplify the task of determining the modal properties of biphotons. In the present paper we provide a theoretical description of SET valid for any quadratic coupling regime between a nonlinear medium and pump fields generating photons by pairs in the low-gain regime. We use our results to obtain not only information about the associated modal function modulus but also its phase, for any mode, and we discuss the specific case of time-frequency variables as well as the quantities and limitations involved in the measurement resolution.

DOI: 10.1103/PhysRevA.106.063709

I. INTRODUCTION

Photons are elementary excitations of the electromagnetic field in a given mode, which can combine polarization, frequency, and transverse position or momentum, among other degrees of freedom. As such, photons cannot be separated from the properties defined by the modes they occupy. This is actually good news: Since modes can be decomposed in an orthonormal basis, they can be manipulated and engineered using linear and nonlinear devices and different modes can be measured independently. Consequently, modes can be used not only to distinguish, isolate, and manipulate quantum properties of the electromagnetic field but also to measure its statistics [1,2].

The interplay between the electromagnetic-field states and modes—or, more poetically, between light and color, if one refers to frequency modes—presents thus many facets, and modes are valuable tools to exploit different properties and aspects of the electromagnetic field. One example is nonlocality tests using single photons, which rely on the independent measurement of the polarization modes of the quantum state of a photon pair in spatially separated modes. The correlations between polarization measurements of photons belonging to the same pair led to the demonstration of nonclassical effects that are particular to quantum states of the field [3].

Polarization, as well as all modal attributes, is a property of the electromagnetic field which applies to both classical and quantum descriptions. The modal measurement statistics inherit the photon's quantum properties and can be used as a way to reveal different surprising aspects of quantum physics such as (in the case of Ref. [3]) nonlocality. In addition, mode manipulation and engineering can lead, through the same principles, to the modification of the photon statistics in particular measurements, controlling, for instance, the distinguishability between photons and tailoring effective commutation relations [4–6].

For photon pairs generated by parametric processes, such as spontaneous parametric down-conversion (SPDC) or four-wave mixing, the modal structure of the photon pair is crucial to infer some quantum properties of the produced state such as entanglement. The conservation laws involved in the photon pair production lead to a correlated joint modal function and the number of independent orthogonal modes which are necessary to describe the pair's mode structure is directly related to the degree of entanglement of the state [7]. Consequently, experimentally inferring entanglement and using it as a resource demand perfect knowledge of the joint modal structure of the photon pair [8].

Finally, the manipulation of the mode basis of squeezed states can transform entangled states into separable ones and vice versa, and this mode basis transformation enables multimode entanglement detection in continuous variables and their applications as quantum teleportation [9]. Modes also play a key role in quantum state measurement and metrology [8,10], since usual techniques such as homodyne detection require a nearly perfect mode overlap between the probed state and the reference state in order to be reliable [11–13].

The mode structure of a quantum field depends on the conditions of its generation, such as the properties of the medium producing it and the complex amplitude of auxiliary fields. One of the simplest configurations leading to the generation of nonclassical states of light consists of nonlinear interactions that can be described by nondegenerate quadratic operators with a complex mode structure

$$\hat{S} = \gamma \iint L(\mathbf{k}, \mathbf{k}')\hat{a}_s^\dagger(\mathbf{k})\hat{a}_i^\dagger(\mathbf{k}')d\mathbf{k}\,d\mathbf{k}'. \tag{1}$$

In the physical process associated with Eq. (1), photons are created in pairs and distributed in different auxiliary modes (as polarization or propagation direction), which are labeled s and i, for signal and idler, with $\iint |L(\mathbf{k}, \mathbf{k}')|^2 d\mathbf{k}\, d\mathbf{k}' = 1$. We choose to discuss the nondegenerate case for generality, but our results also apply to the degenerate case. The modal variables $\mathbf{k}$ and $\mathbf{k}'$ can refer to any mode such as frequency, time, and propagation direction, among others. Also, the integral over modes $\mathbf{k}$ and $\mathbf{k}'$ for the signal and the idler fields may as well involve a sum over discrete modes, such as the orbital angular momentum or polarization. We use only the integral form to simplify the notation.

In Eq. (1), γ is a coupling constant, given by the product of two physically independent quantities, which we label $\mathcal{A}$ and χ, so we can write $\gamma = \mathcal{A}\chi$. While $\mathcal{A}$ depends on physical parameters that can be controlled at each run of an experiment, such as the complex amplitude of auxiliary fields, χ relates to the gain and is considered as a constant in time related only the nonlinear device used in the experiment, such as the material's size and geometry. The distinction between the two parameters is important since in the present paper we always consider that $|\chi|^2 \ll 1$ (see Appendix A), while γ is arbitrary.

Equation (1) can describe different physical processes, such as four-wave mixing, or a general parametric process, for instance. In both of cases mentioned, Eq. (1) is an approximation of the nonlinear interaction describing the conversion of photons from classical fields (coherent states), called pump(s), into two photons, mediated by a material medium. The complete derivation of Eq. (1) can be found in Appendix A and involves considering that the pump's state remains a coherent state (continuous wave or pulsed) and can be treated as classical during its interaction with the medium. This assumption is important since, in this case, Eq. (1) leads to an output quantum state $|\psi_{\text{out}}\rangle$ that can be written, in the low-gain regime, as (see Appendix A)

$$|\psi_{\text{out}}\rangle = e^{\hat{S}-\text{H.c.}}|\psi_{\text{in}}\rangle = \hat{U}|\psi_{\text{in}}\rangle, \tag{2}$$

where $|\psi_{\text{in}}\rangle$ is the total state of the electromagnetic field before the nonlinear interaction.

If $\gamma \ll 1$ (which is the case, for instance, in SPDC), we can consider only the first terms of the expansion of Eq. (2) in powers of γ; in this regime, the creation of photon pairs can be observed by postselection using coincidence detection. Alternatively, but still in the low-gain regime, cavity effects can enhance the creation of squeezed states, which typically can be detected using homodyne detection. These two regimes are contemplated in the present paper, which has as its main goal the measurement of the modal function $L(\mathbf{k}, \mathbf{k}')$. This function is determined by the medium and by the (possible) auxiliary fields' spectral properties, but does not depend on the auxiliary or on the pump field's amplitude.

Hence, from Eq. (2) we see that if $|\psi_{\text{in}}\rangle$ is Gaussian, $|\psi_{\text{out}}\rangle$ will also be Gaussian. If the low-gain hypothesis no longer holds, time-ordering effects must be considered to obtain the evolution operator associated with the nonlinear interaction; this regime was extensively discussed in [14–17].

The tomography of the modal function $L(\mathbf{k}, \mathbf{k}')$ for any mode $\mathbf{k}$ or $\mathbf{k}'$ is a challenging task. Several experimental methods have been proposed according to the specific type of mode one wants to access as well as the coupling strength regime. A good overview of the existing techniques can be found in [18]. Among these, an interesting approach is stimulated emission tomography (SET). Introduced in [19], SET was used with great success to infer mode properties of photon pairs using relatively simple experimental techniques avoiding coincidence counts and low intensity signals, and consequently improving the measurement resolution and reducing the integration time. Stimulated emission tomography can be applied to all types of modes, and its main principles are sketched in Fig. 1: A pump beam is sent through a nonlinear medium, together with a seed beam in mode i. In its original formulation, the seed beam is prepared in a coherent state in a mode defined by $\mathbf{k}_i'$ in support of the idler's mode with resolution $\delta\mathbf{k}'$, where $\delta\mathbf{k}'$ is much narrower that the idler mode's width. Then the intensity of the signal mode is detected with a resolution $\delta\mathbf{k}_s$ around a given value $\mathbf{k}_s$. The main result of [19] was to show that the obtained intensity is proportional to the coincidence detection of photon pairs that are produced in the spontaneous regime, i.e., in the absence of a seed beam. The proportionality factor is given by the intensity of the seed beam, and this is the reason for the signal to noise improvement. Also, since the intensity of the seed beam is known, one can easily recover from this measurement the absolute value of the modal function of the produced two-mode state, $|L(\mathbf{k}_s, \mathbf{k}_i')|^2$ at points $\mathbf{k}_s$ and $\mathbf{k}_i'$ defined by the seed mode choice and the signal beam mode selective detection.

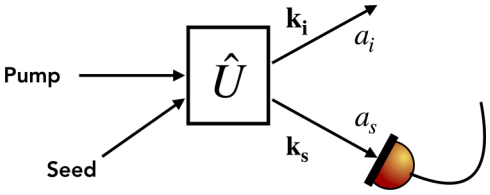

FIG. 1. Schematic of the stimulated emission tomography.

Using SET to obtain full phase and amplitude information about the modal function associated with the signal and idler beams requires different experimental resources according to the mode one is interested in. Stimulated emission tomography can be straightforwardly used to completely characterize the polarization state generated in a nonlinear process [20], since by changing the polarization of the seed beam and the one of the detected signal field one can reconstruct the full two-photon polarization state with intensity measurements only. This idea can be extended to other degrees of freedom, such as propagation direction, by discretizing them, as it was done in [21].

For the field's spectral properties, the situation is trickier. It is experimentally challenging to manipulate and shape the seed to provide information about the phase of the spectral function with intensity measurements only. A clever solution for this was provided in [22], where the authors used the same classical beam as for a pump and seed and as a phase reference pulse. The original field is decomposed, multiplexed, and chirped, and the field generated through the nonlinear interaction is made to interfere with the reference beam with a phase difference that can be experimentally adjusted. The detected signal has the same form as one of the outputs of an

interferometer, so by combining output signals with different phase choices, one reaches a result which is proportional to the photon pair's joint spectral amplitude (JSA) $L(\mathbf{k},\mathbf{k}') = L(\omega,\omega')$. Also, in [23] a on-chip ring interferometer was designed to recover phase information of the stimulated field in a regime where the spectrum of the output stimulated field does not asymptotically reproduce the spectrum of the stimulated photon of the pair. Finally, alternative techniques to obtain phase information [24] and complement the SET measurement in its original formulation were also proposed and implemented in [25–27], but they require using coincidence measurements as well.

In the present paper we present a way to extend the SET technique so it can provide, for arbitrary modes, full information about the produced field's modal function without the need to perform coincidence detection. This means that we show it is possible to obtain information about not only the absolute value of the modal function, as in [19], but also its phase, for any mode. In order to do so, we present a theoretical model for the output field produced by the nonlinear interaction slightly different from the one used, for instance, in [19,28,29]. Furthermore, we consider the exact output state for an arbitrary effective coupling regime [arbitrary value of γ in Eq. (1)]. Finally, we combine the stimulated output field in both signal and idler modes using an interferometric configuration and compute the difference of intensities of the combined modes. The reasons for these modifications are twofold. First of all, since SET relies on classical intensity measurements, all the involved operations, interactions, and elements are Gaussian. Thus, using any step of the model non-Gaussian states may be confusing and inaccurate. The output state in the SET configuration is Gaussian and must be considered as such, in spite of the fact that the spontaneous regime combined with postselection by coincidence detection produces a non-Gaussian state, as is usually the case in SPDC. Second, keeping the full evolution operator in Eq. (2) enables extending SET to other experimental situations where multimode squeezed states can be produced and measured, for instance, optical parametric oscillators and homodyne detection. We will see how these modifications change the results obtained in [19], which can also be recovered by making an expansion on parameters that surprisingly depend not only on the coupling strength but also on the frequency correlation properties of the output field.

We will thus present in the following the exact calculation of the signal intensity detection in the stimulated regime, using methods similar to the ones of [19,28,30]. In addition, we will use our results to propose a method to interferometrically measure either the full modal function, including phase information, or its Fourier transform, according to the choice made on the seed's spectral properties. We will see that the conditions on the seed's spectrum to unveil the modal function or its Fourier transform are not exactly the same as in [19,22] nor are they simply the Fourier analogs to them. They are rather the analog of a two-party spectral homodyne detection.

The paper is organized as follows. Section II is devoted to the direct detection of the signal field, in the same spirit as the original formulation of SET. This section is important to fix notation and establish the main differences between our approach and the one of [19]. In Sec. III we use the obtained results to develop the principles of the interferometric detection. In Sec. IV we discuss the particular case of frequency and time measurements. We briefly summarize in Sec. V.

II. DIRECT DETECTION

The first measurement configuration we study is the same as in the original paper [19] but with a slightly different approach. First of all, we consider that the nonlinear interaction between the medium and the pump beam can be described by the unitary operator appearing in Eq. (2).

The unitary operator is thus applied to the system's initial state $|\psi_{\text{in}}\rangle$, given by the vacuum state displaced by the seed, which is a coherent state $|\psi_o\rangle = \hat{D}(\alpha)|0\rangle$, where α is the complex amplitude of a coherent state in the seed's mode (see Appendix A for a derivation). The seed mode α can also be represented as a superposition of modes. More specifically, the associated multimode displacement operator is given by

$$\hat{D}(\alpha) = \exp\left(\int [\hat{a}^\dagger(\mathbf{k})\alpha(\mathbf{k}) - \hat{a}(\mathbf{k})\alpha^*(\mathbf{k})]d\mathbf{k}\right), \tag{3}$$

where $|\alpha|^2 = \int |\alpha(\mathbf{k})|^2 d\mathbf{k}$. Thus, the state obtained by the application of Eq. (2) to the seeded state $|\psi_o\rangle$ is given by

$$|\psi\rangle = \hat{U}\hat{D}(\alpha)|0\rangle. \tag{4}$$

As we can see in Appendix A, this expression can be obtained using the asymptotic treatment of [30], with no other assumption than the undepleted pump regime, which is justified when $|\chi|^2 \ll 1$ (recall that $\gamma = \mathcal{A}\chi$).

We can now rewrite the operators appearing in Eq. (4) as $\hat{D}(\alpha)\hat{D}^\dagger(\alpha)\hat{U}\hat{D}(\alpha)|0\rangle$ and consider that the seed's mode is orthogonal to the signal's. As a result, the former does not affect the latter and

$$\hat{D}^\dagger(\alpha)\hat{U}\hat{D}(\alpha) = \tilde{\hat{U}} = \exp\left(\gamma \iint L(\mathbf{k},\mathbf{k}')\hat{a}_s^\dagger(\mathbf{k}) \times [\hat{a}_i^\dagger(\mathbf{k}') + \alpha(\mathbf{k}')]d\mathbf{k}\, d\mathbf{k}' - \text{H.c.}\right). \tag{5}$$

If the signal mode is detected close to a given value $\mathbf{k}_s'$, with a measurement resolution $\delta\mathbf{k}_s'$, the intensity of the detected signal can be expressed as

$$\langle \hat{a}_s^\dagger(\mathbf{k}_s')\hat{a}_s(\mathbf{k}_s')\rangle \delta\mathbf{k}_s' = \langle 0|\tilde{\hat{U}}^\dagger \hat{a}_s^\dagger(\mathbf{k}_s')\hat{a}_s(\mathbf{k}_s')\tilde{\hat{U}}|0\rangle \delta\mathbf{k}_s', \tag{6}$$

where we have used that $[\hat{a}(\mathbf{k}_s), \hat{a}^\dagger(\mathbf{k}_i')] = 0$ and that the displacement operator associated with the seed commutes with the signal modes.

It is now convenient to express all the creation and annihilation operators using the Schmidt decomposition. We have then that $\hat{S} = \gamma \iint L(\mathbf{k},\mathbf{k}')\hat{a}_s^\dagger(\mathbf{k})\hat{a}_i^\dagger(\mathbf{k}')d\mathbf{k}\, d\mathbf{k}' = \gamma \sum_n \sqrt{\lambda_n}\hat{b}_n^\dagger \hat{c}_n^\dagger$, where $\hat{b}_n^\dagger = \int \psi_n(\mathbf{k})\hat{a}_s^\dagger(\mathbf{k})d\mathbf{k}$ and $\hat{c}_n^\dagger = \int \phi_n(\mathbf{k})\hat{a}_i^\dagger(\mathbf{k})d\mathbf{k}$ are the Schmidt modes (see Appendix B and [31], for instance, for the full details of the change to the Schmidt basis).

Using the previous results and definitions, we can thus expand, in first place, the operator $\hat{a}(\mathbf{k}_s)$ in the Schmidt basis as

$$\hat{a}_s(\mathbf{k}_s) = \sum_n \psi_n(\mathbf{k}_s)\hat{b}_n. \tag{7}$$

Equivalently, the seed mode $\hat{s} = \int \frac{\alpha^*(\mathbf{k})}{|\alpha|^2}\hat{a}_i(\mathbf{k})d\mathbf{k} = \sum_n \alpha_n^* \hat{c}_n$ can also be expressed in this same basis for convenience, with $\alpha_n = \int \frac{\alpha(\mathbf{k})}{|\alpha|^2}\phi_n^*(\mathbf{k})d\mathbf{k}$ or, alternatively, $\alpha(\mathbf{k}) = |\alpha|^2 \sum_n \alpha_n \phi_n(\mathbf{k})$. Using the Schmidt decomposition, we can now express $\hat{U}^\dagger \hat{a}_s(\mathbf{k}_s)\hat{U}$ as

$$\hat{U}^\dagger \hat{a}_s(\mathbf{k}_s)\hat{U} = \sum_n \psi_n(\mathbf{k}_s)[\hat{b}_n \cosh(\gamma\sqrt{\lambda_n}) + \hat{c}_n^\dagger \sinh(\gamma\sqrt{\lambda_n})] \tag{8}$$

and consequently

$$\begin{aligned}\langle \hat{U}^\dagger \hat{a}_s^\dagger(\mathbf{k}_s)\hat{a}_s(\mathbf{k}_s)\hat{U}\rangle &= \langle 0|\hat{U}^\dagger \hat{a}_s^\dagger(\mathbf{k}_s)\hat{a}_s(\mathbf{k}_s)\hat{U}|0\rangle \\ &= \sum_n |\psi_n(\mathbf{k}_s)|^2 \sinh^2(\gamma\sqrt{\lambda_n}).\end{aligned} \tag{9}$$

We now consider the effect of the seed mode. It performs the transformation $\hat{c}_n \to \hat{c}_n + \alpha_n$ so that Eq. (9) finally becomes

$$\begin{aligned}\langle \hat{U}^\dagger \hat{a}_s^\dagger(\mathbf{k}_s)\hat{a}_s(\mathbf{k}_s)\hat{U}\rangle = &\sum_n |\psi_n(\mathbf{k}_s)|^2 \sinh^2(\gamma\sqrt{\lambda_n}) \\ &+|\alpha|^2\left|\sum_n \alpha_n^* \psi_n(\mathbf{k}_s)\sinh(\gamma\sqrt{\lambda_n})\right|^2,\end{aligned}$$

which is the output of the produced two-mode (signal and idler) field.

We can now discuss Eq. (10). By considering, for instance, that no mode selection is performed and detection is made in the signal mode, we have that the detected intensity can be expressed as $\langle \hat{n}_s\rangle = \langle 0|\hat{n}_s|0\rangle = \int \langle \hat{U}^\dagger \hat{a}_s(\mathbf{k}_s)^\dagger \hat{a}_s(\mathbf{k}_s)\hat{U}\rangle d\mathbf{k}_s$, which leads to

$$\langle \hat{n}_s\rangle = \sum_n \sinh^2(\gamma\sqrt{\lambda_n})(1 + |\alpha_n|^2|\alpha|^2). \tag{10}$$

For $|\alpha|^2 \gg 1$, the first term on the right-hand side of Eq. (10) corresponds to the spontaneous emission term and can be neglected. Also, we have that $\langle \hat{n}_s\rangle \approx \sum_n \sinh^2(\gamma\sqrt{\lambda_n})|\alpha_n|^2|\alpha|^2$. A first consequence of this expression is that by shaping the seed beam only to a Schmidt mode, using techniques similar to the ones proposed in [32], one can measure λ_n and infer the noise and entanglement properties of the whole system.

We now consider, as in [19] and Eq. (6), that the detection is performed in a given mode $\mathbf{k}_s$ in the interval $\delta\mathbf{k}_s$ of the signal mode. Equation (10) then becomes

$$\langle \hat{U}^\dagger \hat{a}_s^\dagger(\mathbf{k}_s)\hat{a}_s(\mathbf{k}_s)\hat{U}\rangle = |\alpha|^2\left|\sum_n \alpha_n^* \psi_n(\mathbf{k}_s)\sinh(\gamma\sqrt{\lambda_n})\right|^2. \tag{11}$$

Several interesting specific cases can be studied from the expression above. If $\gamma\sqrt{\lambda_n} \ll 1$, we have that $\sinh(\gamma\sqrt{\lambda_n}) \approx \gamma\sqrt{\lambda_n}$. In addition, to obtain an expression which is valid for an arbitrary high value of γ, the benefit of the exact expression (11) is to give precise physical insight into the conditions of validity of the usual $\gamma \ll 1$ approximation. Indeed, we see that it is actually the factor $\gamma\lambda_n$ that plays the role of the control parameter. We thus can infer that the usual $\gamma \ll 1$ approximation can remain valid even with a higher pump field intensity if its spectrum and the nonlinear interaction are such that the output field is highly entangled. Indeed, as the number of entangled modes increases, the number of nonzero values of the λ_n parameter also increases, always keeping $\sum_n \lambda_n = 1$. Note that this aspect will not be discussed in detail in the present work.

Now, using that $\sqrt{\lambda_n}\psi_n(\mathbf{k}) = \int L(\mathbf{k},\mathbf{k}')\phi_n^*(\mathbf{k}')d\mathbf{k}'$, we have finally that Eq. (11) becomes

$$\begin{aligned}&\left|\gamma \sum_n \iint L(\mathbf{k}_s,\mathbf{k}')\alpha(\mathbf{k}'')\phi_n(\mathbf{k}'')\phi_n^*(\mathbf{k}')d\mathbf{k}'d\mathbf{k}'\right|^2 \\ &\quad = \left|\gamma \int L(\mathbf{k}_s,\mathbf{k}')\alpha^*(\mathbf{k}')d\mathbf{k}'\right|^2.\end{aligned} \tag{12}$$

If $\alpha(\mathbf{k}')$ has a flat spectrum in support of $L(\mathbf{k}_s,\mathbf{k}')$, we have that Eq. (12) returns the marginal of $L(\mathbf{k}_s,\mathbf{k}')$ with respect to the idler mode. For $\alpha(\mathbf{k}') \approx \delta(\mathbf{k})|\alpha|^2$, so that $|\alpha_n| \approx |\phi_n^*(\mathbf{k})|$, we obtain the original result from [19]:

$$\langle \hat{a}_s^\dagger(\mathbf{k}_s)\hat{a}_s(\mathbf{k}_s)\rangle \approx \gamma^2|\alpha|^2|L(\mathbf{k}_s,\mathbf{k})|^2. \tag{13}$$

We recall that even if from this result one can obtain information about the absolute value of the mode function at each point $\mathbf{k}_s$ and $\mathbf{k}$ it is not obvious to obtain information about the phase of the function $L(\mathbf{k}_s,\mathbf{k})$ for any mode. In order to solve this problem, we now use the output state (4) as the input of an interferometer.

III. INTERFEROMETRIC DETECTION

In this section we use the results obtained in the preceding section in a configuration which leads to the direct measurement of the full joint modal function $L(\mathbf{k},\mathbf{k}')$ of signal and idler beams. For this we assume that the signal and the idler fields are spatially separated and serve as the inputs of an interferometer. Then the two modes are combined in a balanced beam splitter and the intensities of the output fields in modes A and B are detected.

The field operators in the input modes s and i are combined as $\hat{a}_A(\mathbf{k}) = [\hat{a}_s(\mathbf{k}) + \hat{a}_i(\mathbf{k})]/\sqrt{2}$ and $\hat{a}_B(\mathbf{k}) = [\hat{a}_s(\mathbf{k}) - \hat{a}_i(\mathbf{k})]/\sqrt{2}$. The difference between the field intensities detected at each one of the two output ports of the interferometer can be expressed as

$$\begin{aligned}\langle(\hat{N}_A - \hat{N}_B)\rangle &= \int \langle[\hat{a}_A^\dagger(\mathbf{k})\hat{a}_A(\mathbf{k}) - \hat{a}_B^\dagger(\mathbf{k})\hat{a}_B(\mathbf{k})]\rangle d\mathbf{k} \\ &= \int \langle[\hat{a}_s^\dagger(\mathbf{k})\hat{a}_i(\mathbf{k}) + \hat{a}_i^\dagger(\mathbf{k})\hat{a}_s(\mathbf{k})]\rangle d\mathbf{k},\end{aligned} \tag{14}$$

which is thus the measurement of the nonresolved modal cross correlation of the signal and idler fields.

We can now use the Schmidt decomposition of Eq. (1) and of the idler mode to compute the effect of the nonlinear evolution operator on $\hat{a}_i(\mathbf{k})$:

$$\hat{U}^\dagger \hat{a}_i(\mathbf{k})\hat{U} = \sum_n \phi_n(\mathbf{k})[\hat{c}_n \cosh(\gamma\sqrt{\lambda_n}) + \hat{b}_n^\dagger \sinh(\gamma\sqrt{\lambda_n})]. \tag{15}$$

Then, considering as before the effect of the seed field, which displaces the idler mode, we have that Eq. (14)

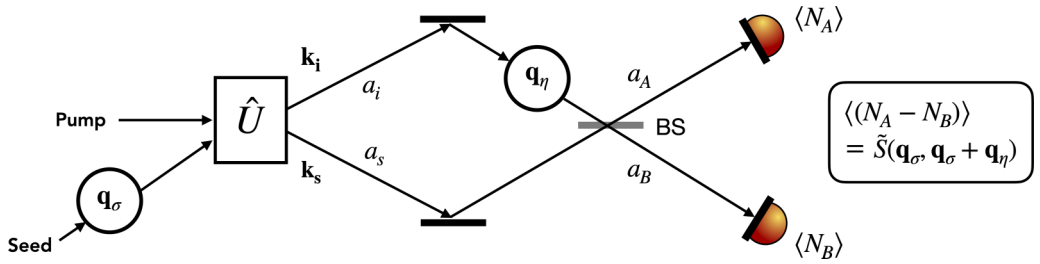

FIG. 2. Interferometric detection for the joint temporal amplitude. In the time-frequency case, the parameters are $q_\sigma \equiv \tau$ and $q_\eta \equiv t$ and BS stands for beam splitter. A classical pump field and a coherent seed field generate a pair of modes denoted by a_i and a_s. The seed is shifted by q_σ before the stimulated emission process, and the output mode is then shifted from a value q_η. The two modes a_i and a_s are then recombined into a balanced beam splitter, and nonresolved direct detections are performed in each final mode a_A and a_B.

becomes

$$\langle (\hat{N}_A - \hat{N}_B) \rangle = |\alpha|^2 \mathrm{Re}\left[\int \sum_{n,m} \psi_n^*(\mathbf{k}) \phi_m(\mathbf{k}) \alpha_n \alpha_m \sinh(2\gamma\sqrt{\lambda_n}) d\mathbf{k} \right]. \tag{16}$$

It is now convenient to reexpress Eq. (16) by transforming the seed mode back from the Schmidt decomposition. By doing so, we can study, for instance, the limit $\gamma \ll 1$, which can be written as

$$\langle (\hat{N}_A - \hat{N}_B) \rangle = 2\,\mathrm{Re}\left[\iint \gamma L(\mathbf{k}, \mathbf{k}') \alpha^*(\mathbf{k}) \alpha^*(\mathbf{k}') d\mathbf{k}\, d\mathbf{k}' \right]. \tag{17}$$

Our first comment on Eq. (17) is that even though it relates to the real part of a function, one can easily access the imaginary part of this function by simply changing the phase of the signal (or the idler) beam, which can be done with standard experimental techniques. One example is by adding a delay line [33] or a spatial light modulator [34] in the mode of the signal beam before it reaches the beam splitter. By doing so, the beam-splitter input mode corresponding to the signal beam acquires a phase difference of $\pi/2$ with respect to the one corresponding to the idler beam. Alternatively, one can impinge an extra $\pi/4$ phase difference between the seed beam and the pump so that the cumulated phase in the integrand is $\pi/2$ shifted with respect to (17).

We can see that Eq. (17) does not provide full information about the modal function $L(\mathbf{k}, \mathbf{k}')$. Nevertheless, studying some particular cases can be helpful to gain some intuition and find out how to experimentally access this function.

To start with, let us suppose that the seed field's modal distribution is much broader than the width of the function $L(\mathbf{k}, \mathbf{k}')$ and that it is nearly flat in the region of the support of $L(\mathbf{k}, \mathbf{k}')$. In this case, we can take the seed out of the integral in Eq. (17), which becomes

$$\begin{aligned} \langle (\hat{N}_A - \hat{N}_B) \rangle &= 2\,\mathrm{Re}\left[\gamma \mathcal{B}^2 \iint L(\mathbf{k}, \mathbf{k}') d\mathbf{k}\, d\mathbf{k}' \right] \\ &= 2\,\mathrm{Re}[\gamma \mathcal{B}^2 \tilde{L}(0,0)], \end{aligned} \tag{18}$$

where $\tilde{L}(\mathbf{q}, \mathbf{q}') = \iint L(\mathbf{k}, \mathbf{k}') e^{i\mathbf{q}\mathbf{k}} e^{i\mathbf{q}'\mathbf{k}'} d\mathbf{k}\, d\mathbf{k}'$ is the Fourier transform of the function $L(\mathbf{k}, \mathbf{k}')$ and $\mathcal{B}$ is the value of the amplitude of the seed which is taken as a constant for $\mathbf{k}$ and $\mathbf{k}'$ in support of $L(\mathbf{k}, \mathbf{k}')$.

Equation (18) provides information about only one point of the modal distribution's Fourier transform, given by $\mathbf{q} = \mathbf{q}' = 0$. Of course this is not enough to completely characterize the modal state of the produced field. Accessing the whole modal function's Fourier transform requires measuring all the points of the function $\tilde{L}(\mathbf{q}, \mathbf{q}')$. In order to do so, we will adapt the interferometer as depicted in Fig. 2.

We first apply a phase difference between the two arms of the interferometer and, say, the idler mode is transformed as $\hat{a}_i(\mathbf{k}) \to \hat{U}^\dagger_{\mathbf{q}_\eta} \hat{a}_i(\mathbf{k}) \hat{U}_{\mathbf{q}_\eta}$, where $\hat{U}^\dagger_{\mathbf{q}_\eta}$ is the unitary operator that implements a phase difference between the two arms of the interferometer. This phase can be considered to be proportional to a parameter $\mathbf{q}_\eta$. By choosing $\hat{U}_{\mathbf{q}_\eta}$ such that $\hat{U}^\dagger_{\mathbf{q}_\eta} \hat{a}_i(\mathbf{k}) \hat{U}_{\mathbf{q}_\eta} = e^{i\mathbf{k}\mathbf{q}_\eta} \hat{a}_i(\mathbf{k})$, it is easy to check that Eq. (17) becomes

$$\langle (\hat{N}_A - \hat{N}_B) \rangle = 2\,\mathrm{Re}\left[\gamma \iint L(\mathbf{k}, \mathbf{k}') \alpha^*(\mathbf{k}) \alpha^*(\mathbf{k}') e^{i\mathbf{k}'\mathbf{q}_\eta} d\mathbf{k}\, d\mathbf{k}' \right]. \tag{19}$$

We can now add another phase factor, but this time to the seed pulse and *before* it interacts with the nonlinear medium. This corresponds to providing a relative phase factor of $\mathbf{q}_\sigma$ between the seed and the pump beam so that $\alpha(\mathbf{k}) \to \alpha(\mathbf{k}) e^{-i\mathbf{k}\mathbf{q}_\sigma}$. The complete measurement scheme is represented in Fig. 2, where all the phase factors are identified. It consists of a configuration analogous to the one implemented in [35,36], where it is shown that transformations implemented on the seed's transverse field profile are transferred to the signal's.

The produced output signal is then given by

$$\begin{aligned} \langle (\hat{N}_A - \hat{N}_B) \rangle &= 7\tilde{S}(\mathbf{q}_\sigma, \mathbf{q}_\sigma + \mathbf{q}_\eta) \\ &= 2\,\mathrm{Re}\left[\gamma \iint L(\mathbf{k}, \mathbf{k}') \alpha^*(\mathbf{k}) e^{i\mathbf{k}\mathbf{q}_\sigma} \right. \\ &\quad \left. \times \alpha^*(\mathbf{k}') e^{i\mathbf{k}'\mathbf{q}_\sigma} e^{i\mathbf{k}'\mathbf{q}_\eta} d\mathbf{k}\, d\mathbf{k}' \right], \end{aligned} \tag{20}$$

where $\tilde{S}(\mathbf{q}_1, \mathbf{q}_2)$ is the Fourier transform of the function $L(\mathbf{k}_1, \mathbf{k}_2) \alpha^*(\mathbf{k}_1) \alpha^*(\mathbf{k}_2)$. As before, we first discuss the situation of a seed beam with a broad and flat modal distribution,

which leads directly to

$$\langle(\hat{N}_A - \hat{N}_B)\rangle = \tilde{L}(\mathbf{q}_\sigma, \mathbf{q}_\sigma + \mathbf{q}_\eta) = 2\,\mathrm{Re}\left[\gamma\mathcal{B}^2 \iint L(\mathbf{k}, \mathbf{k}')e^{i\mathbf{k}\mathbf{q}_\sigma} e^{i\mathbf{k}'\mathbf{q}_\sigma} e^{i\mathbf{k}'\mathbf{q}_\eta} d\mathbf{k}\, d\mathbf{k}'\right]. \tag{21}$$

The function $\tilde{L}(\mathbf{q}_\sigma, \mathbf{q}_\sigma + \mathbf{q}_\eta)$ is the Fourier transform of the modal function $L(\mathbf{k}, \mathbf{k}')$ at points $\mathbf{q}_\sigma$ and $\mathbf{q}_\sigma + \mathbf{q}_\eta$. As a consequence, once the real part of $\tilde{L}(\mathbf{q}_\sigma, \mathbf{q}_\sigma + \mathbf{q}_\eta)$ is also measured, the proposed scheme enables the complete measurement of the modal function $L(\mathbf{k}, \mathbf{k}')$ and/or its Fourier transform, including its phase information. We can see that the required modal properties of the seed are opposite to the ones used in the direct detection configuration. While in that case the seed was supposed to have a narrow modal distribution, in the present one we consider it to have a broad, nearly flat one. This is somehow intuitive, since in the direct detection configuration we accessed the absolute value of the function $L(\mathbf{k}, \mathbf{k}')$, while in the interferometric setup we can measure its Fourier transform $\tilde{L}(\mathbf{q}_\sigma, \mathbf{q}_\sigma + \mathbf{q}_\eta)$.

We now mention a second method to extract the spectrum $L(\mathbf{k}, \mathbf{k}')$ which loosens the assumptions about the temporal width of the idler beam. We suppose that the seed beam is known, since it can be independently measured completely with tomography techniques, such as the ones described in [37–39]. Then if we measure both real and imaginary parts of the signal, we obtain the function

$$\tilde{S}(\mathbf{q}_\sigma, \mathbf{q}_\eta + \mathbf{q}_\sigma) = 2\gamma \iint L(\mathbf{k}, \mathbf{k}')\alpha^*(\mathbf{k}') \times \alpha^*(\mathbf{k})e^{i\mathbf{k}\mathbf{q}_\sigma} e^{i\mathbf{k}'\mathbf{q}_\eta} e^{i\mathbf{k}'\mathbf{q}_\sigma} d\mathbf{k}\, d\mathbf{k}'. \tag{22}$$

By performing a double Fourier transform on the obtained function and dividing it by the (known) spectrum of the seed beam, we obtain the spectrum of interest

$$L(\mathbf{k}, \mathbf{k}') = \frac{1}{8\pi^2\gamma} \frac{\iint \tilde{S}(\mathbf{q}_\sigma, \mathbf{q}_\sigma)e^{-i\mathbf{k}\mathbf{q}_\sigma} e^{-i\mathbf{k}'\mathbf{q}_\eta} e^{-i\mathbf{k}'\mathbf{q}_\sigma} d\mathbf{k}\, d\mathbf{k}'}{\alpha^*(\mathbf{k}')\alpha^*(\mathbf{k})}, \tag{23}$$

thus providing a direct measurement of the modal function at all points.

We have presented a general method to directly measure the function $L(\mathbf{k}, \mathbf{k}')$. The proposed solution provides all the modal properties associated with the field produced by a quadratic interaction between a nonlinear medium and a pump beam in the low-gain regime using intensity measurements only, circumventing coincidence measurements. We notice that errors due to expansion on γ depend on γ^3. A discussion about precision and sampling requirements and the effects of noise and measurement imperfections can be found in Appendix C.

The description and discussion presented apply to any degree of freedom of the electromagnetic field in the low-gain regime and in the undepleted pump approximation. In the next section we will discuss in detail the case of frequency and time degrees of freedom.

IV. JOINT TEMPORAL AMPLITUDE RECONSTRUCTION

We now study in detail the case of frequency and time modes, which is particularly interesting due to the experimental difficulties in manipulating these degrees of freedom, and thus measuring the modal function in all points with phase information, when compared, for instance, to the polarization or the transverse position and momentum. Also, frequency modes and states have many applications in different experimental setups described by the interaction (2). In the intense pump coupling regime, for instance, it is possible to create multimode squeezed states of the radiation both in the bulk or in the circuit configurations [13,40–43], and the choice of different frequency mode basis adapts the squeezed and highly mode-entangled produced state [44,45] to applications such as quantum metrology, quantum information, and quantum communication.

In the weak-coupling regime, such as the SPDC one, frequency also plays an important role. In this case, the unitary operator (2) is expanded until the first order and the state produced is postselected by coincidence measurements, which excludes the vacuum part of the state. The resulting postselected state becomes a valuable non-Gaussian resource in quantum optics and quantum information. This state can be, for instance, highly entangled in different modes, such as polarization, which can be used to encode qubits, or frequency, which can be used to encode qubits or qudits [46,47] or for continuous variables for quantum computing [48–50] and metrology [51].

In order to analyze the time and frequency mode case, we change the notation so that $L(\mathbf{k}, \mathbf{k}') \equiv L(\omega, \omega')$ and $\tilde{L}(\mathbf{q}_\eta, \mathbf{q}_\sigma) \equiv \tilde{L}(\tau, t)$ are the JSA and the joint temporal amplitude, respectively. In order to do so, we now identify how the different terms appearing in Eq. (20) can be experimentally implemented. The first point to be addressed is the pump's spectral width. By inverting Eq. (20) and using this section's notation, we see that

$$L(\omega, \omega') = \frac{1}{8\pi^2\gamma} \frac{\iint \tilde{S}(\tau, t + \tau)e^{-i\tau\omega} e^{-i(t+\tau)\omega'} dt\, d\tau}{\alpha^*(\omega)\alpha^*(\omega')} \tag{24}$$

can be inferred by varying t and τ and reconstructing $\tilde{S}(\tau, t + \tau)$ from the measurement results. Of course, $\alpha(\omega)$ should be known, and it must have a support larger than the one of $L(\omega, \omega')$; otherwise $\tilde{S}(\tau, t + \tau)$ cannot be reconstructed.

The second point to be discussed is how to implement the temporal delay τ. This term is associated with an optical path difference between the pump and the seed (see Fig. 2). We can assume, for instance, that both the pump and seed come from the same laser and the pump is frequency doubled while the seed is attenuated. In this case, we ensure the phase coherence between both classical beams and the possibility to choose the relative phase proportional to the parameter τ between both wave packets. This time delay between pump and seed beams can occur *before* the nonlinear interaction and is inherited by the photons created by it. This is a situation similar to the one studied in [35] but in the context of the beam's transverse profile. Finally, experimentally, the phase difference proportional to the time delay t can be obtained *after* the nonlinear interaction by placing an optical path difference in the idler's arm, as is usually done in interferometers.

In addition, one cannot determine t and τ with infinite precision. Typical values of the size of each time step are of the order of 0.3 fs (which corresponds to 100 nm of optical path), with a typical precision of 0.03 fs. In [52], for instance, smaller time steps corresponding to an optical path of 30 nm were implemented.

Concerning the pump spectral profile, in the case of a pulsed pump, we can use pump shaping techniques to use a seed beam broader than the pump. Using the numbers of [4], for instance, we can use a laser with 0.5 ps pulse duration for the seed and stretch the impulsions coming from the same laser by a factor of 10 to pump the nonlinear structure; this leads to a seed beam whose spectrum is 10 times larger than the pump's one and consequently the JSA's.

A general discussion of the experimental requirements can be found in Appendix C for arbitrary modes, together with the main idea of how to sample results experimentally.

V. CONCLUSION

We have extended the principles of SET and proposed an interferometric method to obtain full phase information about the modal function $L(\mathbf{k},\mathbf{k}')$ avoiding single-photon coincidence detection. The results obtained are analogous to those for two-dimensional homodyne detection but acting on the mode profile of the field instead of its quadratures. We have discussed in detail the case of the time and spectral properties of the field as well as the role of noise and imperfections (see Appendix C). In addition, the proposed method in principle can also be used to directly infer the JSA from the joint temporal amplitude simply by reversing the roles of frequency and time.

We believe that the present work will be useful for different experimental configurations and setups where the modal properties of the field play a role in quantum information, metrology, and imaging.

APPENDIX A: FIELD QUANTUM STATE GENERATED BY THE NONLINEAR DEVICE

In this Appendix we show that the quantum state of the light $|\psi_{\text{out}}\rangle$ emitted by the nonlinear device can be written as

$$|\psi_{\text{out}}\rangle = \hat{U}|\psi_{\text{in}}\rangle = e^{\hat{S}-\text{H.c.}}|\psi_{\text{in}}\rangle, \tag{A1}$$

where $|\psi_{\text{in}}\rangle$ is the quantum state of the light incident upon the nonlinear device and

$$\hat{S} = \gamma \sum_{\nu,\eta} \int d\vec{k}_1 d\vec{k}_2 L_{\nu,\eta}(\vec{k}_1,\vec{k}_2)\hat{b}^\dagger_{\nu\vec{k}_1}\hat{b}^\dagger_{\eta\vec{k}_2}.$$

In this relation, the couple $(\nu,\vec{k})$ labels a plane-wave mode of the field with wave vector $\vec{k}$ and $\nu=\pm1$ labels the two orthogonal polarization. The function $L_{\nu,\eta}(\vec{k}_1,\vec{k}_2)$ which characterizes the state of the emitted field is such that $\sum_{\nu,\eta}\int d\vec{k}_1 d\vec{k}_2 |L_{\nu,\eta}(\vec{k}_1,\vec{k}_2)|^2 = 1$. The factor γ can be written as $\gamma = \chi\mathcal{A}$, where χ is a characteristic of the nonlinear device and $|\chi|^2$ represents the number of photon pairs generated per photon of the pump pulse. Further, $\mathcal{A}$ is a characteristic of the pump pulse and $|\mathcal{A}|^2$ is the mean number of photons in the pump pulse. Therefore, $|\gamma|^2$ is the total number of photon pairs generated by the pump pulse.

As in Ref. [30] or [19], we consider that the device is characterized by a Hamiltonian $\hat{H}_{\text{L}} + \hat{H}_{\text{NL}}$, where $\hat{H}_{\text{L}}$ collects the linear interactions responsible for the propagation and dispersion and $\hat{H}_{\text{NL}}$ collecting the nonlinear interactions is given by

$$\hat{H}_{\text{NL}} = -\left[\sum_{\nu,\eta,\mu}\int d\vec{k}_1 d\vec{k}_2 d\vec{k} S_{\nu\eta\mu}(\vec{k}_1,\vec{k}_2,\vec{k})\hat{b}^\dagger_{\nu\vec{k}_1}\hat{b}^\dagger_{\eta\vec{k}_2}\hat{a}_{\mu\vec{k}} + \text{H.c.}\right], \tag{A2}$$

where the function $S_{\nu\eta\mu}(\vec{k}_1,\vec{k}_2,\vec{k})$ encompasses the nonlinear coupling and phase-matching condition. We proceed as in Ref. [30], where only the spontaneous process was considered and we generalize to the stimulated case, where the incident field is not necessarily the vacuum. For the sake of self-contentedness, we briefly summarize the methodology which relies on scattering theory and backward propagation. The states $|\psi_{\text{in}}\rangle$ and $|\psi_{\text{out}}\rangle$ are scattering states [30,53]; $|\psi_{\text{in}}\rangle$ is the field state at $t=0$ which develops from $|\psi(t_-)\rangle$ but considering that the nonlinear device has been removed, that is, $|\psi_{\text{in}}\rangle = \exp[-i\hat{H}_{\text{L}}(0-t_-)]|\psi(t_-)\rangle$ (throughout this Appendix we consider $\hbar=1$). In the same way, $|\psi_{\text{out}}\rangle$ is the state at $t=0$ which will develop to $|\psi(t_+)\rangle$, without the nonlinear device, that is, $|\psi(t_+)\rangle = \exp[-i\hat{H}_{\text{L}}(t_+-0)]|\psi_{\text{out}}\rangle$. The times t_- and t_+ are considered as $t_\pm\to\pm\infty$. In that way, the effect of the nonlinear device is completely described by the transition from $|\psi_{\text{in}}\rangle$ to $|\psi_{\text{out}}\rangle$ at $t=0$.

The relation between the in and the out states can be written as

$$|\psi_{\text{out}}\rangle = \lim_{t_\pm\to\pm\infty}\hat{U}(t_+,t_-)|\psi_{\text{in}}\rangle, \tag{A3}$$

where $\hat{U}(t_+,t_-)$ is given by

$$\hat{U}(t_+,t_-) = \exp(i\hat{H}_{\text{L}}t_+)\exp[-i\hat{H}(t_+-t_-)]\exp(-i\hat{H}_{\text{L}}t_-). \tag{A4}$$

The unitary operator $\hat{U}(t_+,t)$, as a function of t, fulfills the differential equation

$$-i\frac{\partial}{\partial t}\hat{U}(t_+,t) = \hat{U}(t_+,t)\hat{V}(t), \tag{A5}$$

with

$$\hat{V}(t) = \exp(i\hat{H}_{\text{L}}t)\hat{H}_{\text{NL}}\exp(-i\hat{H}_{\text{L}}t).$$

Using Eq. (A2), we have

$$V(t) = -\left[\sum_{\nu,\eta,\mu}\int d\vec{k}_1 d\vec{k}_2 d\vec{k} S_{\nu\eta\mu}(\vec{k}_1,\vec{k}_2,\vec{k})\exp[-i(\omega_{\mu\vec{k}} - \omega_{\nu\vec{k}_1} - \omega_{\eta\vec{k}_2})t]\hat{b}^\dagger_{\nu\vec{k}_1}\hat{b}^\dagger_{\eta\vec{k}_2}\hat{a}_{\mu\vec{k}} + \text{H.c.}\right]. \tag{A6}$$

As in Ref. [30], we will use backpropagation (from t_+ to t_-) because our objective is to express expectation value of observables which are written as a function of output mode's annihilation and creation operators (at $t_+\to+\infty$).

Before starting the calculations, let us state the assumptions. We suppose that the function $S_{\nu\eta\mu}(\vec{k}_1, \vec{k}_2, \vec{k})$ characterizing the nonlinear device in Eq. (A2) is nonzero only when the pump $(\mu, \vec{k})$, the signal $(\nu, \vec{k}_1)$, and the idler $(\eta, \vec{k}_2)$ modes satisfy the phase-matching condition imposed by the nonlinear medium and the device geometry. Furthermore, the following assumptions are in order.

(1) The pump mode is orthogonal to the other modes, i.e., the seed, signal, and idler modes. Moreover, the frequency range of the pump mode does not overlap with the other modes.

(2) The seed mode overlaps with the idler mode and is orthogonal to the signal mode.

(3) The probability to emit a photon pair, per pump photon, is very small.

To obtain $|\psi_{\text{out}}\rangle$ using Eq. (A3), we must specify the in state of the field $|\psi_{\text{in}}\rangle$. We consider that before entering the nonlinear device the state of the field is well described by a coherent state, corresponding to the pump and the seed pulse. Because of assumptions 1 and 2, we can write the in state as $|\psi_{\text{in}}\rangle = |\psi_p\rangle \otimes |\psi_s\rangle$, where $|\psi_p\rangle$ refers to the pump pulse coherent state and $|\psi_s\rangle$ to the seed coherent pulse. To describe the field states corresponding to the pump pulse, we first define the creation operator $A[f_p]^\dagger$ as

$$\hat{A}^\dagger[f_p] = \sum_\mu \int f_p(\mu, \vec{k}) \hat{a}^\dagger_{\mu,\vec{k}} d\vec{k}, \tag{A7}$$

where the function $f_p(\mu, \vec{k})$ characterizes the mode of the pump and is normalized as $\sum_\mu \int |f_p(\mu, \vec{k})|^2 d\vec{k} = 1$. The in field state $|\psi_p\rangle$ corresponding to the pump pulse is then written as $|\psi_p\rangle = D[\mathcal{A}, f_p]|\text{vac}\rangle$, where the displacement operator $D[\mathcal{A}, f_p]$ is defined as

$$D[\mathcal{A}, f_p] = \exp(\mathcal{A}A^\dagger[f_p] - \text{H.c.})$$

and $|\mathcal{A}|^2$ is the mean number of photon in the mode f_p, that is, $\langle\psi_p| \sum_\mu \int a^\dagger_{\mu\vec{k}} a_{\mu\vec{k}} d\vec{k} |\psi_p\rangle = |\mathcal{A}|^2$.

The seed pulse coherent state $|\psi_s\rangle$ is defined in the same way but with the help of the normalized mode function $f_s(\mu, \vec{k})$ and the corresponding displacement operator $D[\mathcal{B}, f_s]$ as $|\psi_s\rangle = D[\mathcal{B}, f_s]|\text{vac}\rangle$, where

$$D[\mathcal{B}, f_s] = \exp(\mathcal{B}B^\dagger[f_s] - \text{H.c.}).$$

The creation operator $B^\dagger[f_s]$ is defined as in Eq. (A8) but replacing f_p by f_s:

$$B^\dagger[f_s] = \sum_\mu \int f_s(\mu, \vec{k}) b^\dagger_{\mu,\vec{k}} d\vec{k}. \tag{A8}$$

We have used the denotation $b^\dagger_{\mu,\vec{k}}$ for the creation operators to remember that they commute with the annihilation operator $a_{\mu,\vec{k}}$ because the support of the functions f_s and f_p is orthogonal, $\sum_\mu \int d\vec{k} f_s^*(\mu, \vec{k}) f_p(\mu, \vec{k}) = 0$, by assumption 1.

Finally, the in state is thus written as

$$|\psi_{\text{in}}\rangle = D[\mathcal{A}, f_p] \otimes D[\mathcal{B}, f_s]|\text{vac}\rangle. \tag{A9}$$

Setting $\mathcal{B} = 0$ gives the spontaneous parametric conversion process and when $\mathcal{B} \neq 0$ the stimulated process is considered.

To calculate the out state we follow the work by Yang *et al.* in [30]. Let us define two operators

$$K_a = \mathcal{A}A^\dagger[f_p], \quad K_b = \mathcal{B}B^\dagger[f_s]. \tag{A10}$$

Then

$$\begin{aligned} |\psi_{\text{out}}\rangle &= U(t_+, t_-) e^{K_a - \text{H.c.}} e^{K_b - \text{H.c.}} |\text{vac}\rangle \\ &= U(t_+, t_-) e^{K_a - \text{H.c.}} e^{K_b - \text{H.c.}} U^\dagger(t_+, t_-) |\text{vac}\rangle \\ &= e^{\bar{K}_a(t_-) - \text{H.c.}} e^{\bar{K}_b(t_-) - \text{H.c.}} |\text{vac}\rangle, \end{aligned} \tag{A11}$$

where

$$\hat{\bar{K}}_{a(b)}(t) = \hat{U}(t_+, t) \hat{K}_{a(b)} \hat{U}^\dagger(t_+, t) \tag{A12}$$

and the second equality in Eq. (A11) follows from the fact that $H_{\text{L}}|\text{vac}\rangle = H_{\text{NL}}|\text{vac}\rangle = 0$.

The backpropagated operator $\hat{\bar{K}}_{a(b)}(t)$ satisfies

$$\hat{\bar{K}}_{a(b)}(t) = \hat{U}(t_+, t) \hat{K}_{a(b)} \hat{U}^\dagger(t_+, t) \tag{A13}$$

where $\hat{\bar{V}}(t) = \hat{U}(t_+, t) \hat{V}(t) \hat{U}^\dagger(t_+, t)$. Using Eqs. (A4), (A2), and (A6), it can be written as

$$\hat{\bar{V}}(t) = -\left[\sum_{\nu,\eta,\mu} \int d\vec{k}_1 d\vec{k}_2 d\vec{k} S_{\nu\eta\mu}(\vec{k}_1, \vec{k}_2, \vec{k}) \exp\left[-i(\omega_{\mu\vec{k}} - \omega_{\nu\vec{k}_1} - \omega_{\eta\vec{k}_2})t\right] \hat{\bar{b}}^\dagger_{\nu\vec{k}_1}(t) \hat{\bar{b}}^\dagger_{\eta\vec{k}_2}(t) \hat{\bar{a}}_{\mu\vec{k}}(t) + \text{H.c.} \right], \tag{A14}$$

where the bar above an operator means its backpropagation as in Eq. (A12). In the following it is convenient to distinguish the pump and seed mode annihilation operators as $c_{\mu,\vec{k}}$ and $d_{\mu,\vec{k}}$, respectively. In the following calculation the commutators of these operators can be considered as zero, that is, $[c_{\mu,\vec{k}}, d_{\eta,\vec{k}'}] = [c^\dagger_{\mu,\vec{k}}, d_{\eta,\vec{k}'}] = 0$, because the ranges of $\vec{k}$ and $\vec{k}'$ will never overlap. With this notation $\bar{V}(t)$ can be rewritten as

$$\begin{aligned} \hat{\bar{V}}(t) = &-\left[\sum_{\nu,\eta,\mu} \int d\vec{k}_1 d\vec{k}_2 d\vec{k} S_{\nu\eta\mu}(\vec{k}_1, \vec{k}_2, \vec{k}) \exp\left[-i(\omega_{\mu\vec{k}} - \omega_{\nu\vec{k}_1} - \omega_{\eta\vec{k}_2})t\right] \hat{\bar{b}}^\dagger_{\nu\vec{k}_1}(t) \hat{\bar{b}}^\dagger_{\eta\vec{k}_2}(t) \hat{\bar{c}}_{\mu\vec{k}}(t) + \text{H.c.} \right] \\ &-\left[\sum_{\nu,\eta,\mu} \int d\vec{k}_1 d\vec{k}_2 d\vec{k} S_{\nu\eta\mu}(\vec{k}_1, \vec{k}_2, \vec{k}) \exp\left[-i(\omega_{\mu\vec{k}} - \omega_{\nu\vec{k}_1} - \omega_{\eta\vec{k}_2})t\right] \bar{b}^\dagger_{\nu\vec{k}_1}(t) \hat{\bar{b}}^\dagger_{\eta\vec{k}_2}(t) \hat{\bar{d}}_{\mu\vec{k}}(t) + \text{H.c.} \right]. \end{aligned} \tag{A15}$$

The backpropagated creation and annihilation operators all fulfill the same differential equation as the one fulfilled by $\bar{K}(t)$ given in Eq. (A13). In addition, in the integral we have the commutation relations (see rules 1 and 2)

$$\begin{aligned}&\big[\hat{\bar{c}}_{\mu\vec{k}}(t),\hat{\bar{b}}^{\dagger}_{\nu\vec{k}_1}(t)\big]=\big[\hat{\bar{c}}^{\dagger}_{\mu\vec{k}}(t),\hat{\bar{b}}^{\dagger}_{\nu\vec{k}_1}(t)\big]=\big[\hat{\bar{c}}_{\mu\vec{k}}(t),\hat{\bar{b}}^{\dagger}_{\eta\vec{k}_2}(t)\big]=[\hat{\bar{c}}^{\dagger}_{\mu\vec{k}}(t),\hat{\bar{b}}^{\dagger}_{\eta\vec{k}_2}(t)]=0,\\&\big[\hat{\bar{d}}_{\mu\vec{k}}(t),\hat{\bar{b}}^{\dagger}_{\nu\vec{k}_1}(t)\big]=\big[\hat{\bar{d}}^{\dagger}_{\mu\vec{k}}(t),\hat{\bar{b}}^{\dagger}_{\nu\vec{k}_1}(t)\big]=0.\end{aligned}\tag{A16}$$

The overlap of the seed mode with the idler mode can be characterized by an overlap function $f_{\mu,\mu'}(\vec{k},\vec{k}')$ as

$$\big[\hat{\bar{d}}^{\dagger}_{\mu\vec{k}}(t),\hat{\bar{b}}_{\mu'\vec{k}'}(t)\big]=f_{\mu,\mu'}(\vec{k},\vec{k}').\tag{A17}$$

Therefore, the differential equations fulfilled by $\hat{\bar{c}}^{\dagger}_{\mu\vec{k}}(t)$, $\hat{\bar{d}}^{\dagger}_{\mu\vec{k}}(t)$, and $\hat{\bar{b}}^{\dagger}_{\mu\vec{k}}(t)$ are

$$i\frac{d}{dt}\hat{\bar{c}}^{\dagger}_{\mu\vec{k}}(t)=\sum_{\nu,\eta}\int d\vec{k}_1d\vec{k}_2S_{\nu\eta\mu}(\vec{k}_1,\vec{k}_2,\vec{k})\exp\big[-i\big(\omega_{\mu\vec{k}}-\omega_{\nu\vec{k}_1}-\omega_{\eta\vec{k}_2}\big)t\big]\hat{\bar{b}}^{\dagger}_{\nu\vec{k}_1}(t)\hat{\bar{b}}^{\dagger}_{\eta\vec{k}_2}(t),\tag{A18}$$

$$\begin{aligned}i\frac{d}{dt}\bar{d}^{\dagger}_{\mu\vec{k}}(t)=&\sum_{\nu,\eta,\mu'}\int d\vec{k}_1d\vec{k}_2d\vec{k}'f_{\mu,\eta}(\vec{k},\vec{k}_2)S^{*}_{\nu\eta\mu'}(\vec{k}_1,\vec{k}_2,\vec{k}')\exp\big[i\big(\omega_{\mu'\vec{k}'}-\omega_{\nu\vec{k}_1}-\omega_{\eta\vec{k}_2}\big)t\big]\hat{\bar{c}}^{\dagger}_{\mu'\vec{k}'}(t)\hat{\bar{b}}_{\nu\vec{k}_1}(t)\\&+\sum_{\nu,\eta,\mu'}\int d\vec{k}_1d\vec{k}_2d\vec{k}'f_{\mu,\eta}(\vec{k},\vec{k}_2)S^{*}_{\nu\eta\mu'}(\vec{k}_1,\vec{k},\vec{k}')\exp\big[i\big(\omega_{\mu'\vec{k}'}-\omega_{\nu\vec{k}_1}-\omega_{\eta\vec{k}_2}\big)t\big]\hat{\bar{d}}^{\dagger}_{\mu'\vec{k}'}(t)\hat{\bar{b}}_{\nu\vec{k}_1}(t)\\&+\sum_{\nu,\eta}\int d\vec{k}_1d\vec{k}_2S_{\nu\eta\mu}(\vec{k}_1,\vec{k}_2,\vec{k})\exp\big[-i\big(\omega_{\mu\vec{k}}-\omega_{\nu\vec{k}_1}-\omega_{\eta\vec{k}_2}\big)t\big]\hat{\bar{b}}^{\dagger}_{\nu\vec{k}_1}(t)\hat{\bar{b}}^{\dagger}_{\eta\vec{k}_2}(t),\end{aligned}\tag{A19}$$

$$i\frac{d}{dt}\hat{\bar{b}}^{\dagger}_{\nu\vec{k}_1}(t)=\sum_{\eta,\mu}\int d\vec{k}\,d\vec{k}_2\big[S^{*}_{\nu\eta\mu}(\vec{k}_1,\vec{k}_2,\vec{k})+S^{*}_{\eta\nu\mu}(\vec{k}_2,\vec{k}_1,\vec{k})\big]\exp\big[i\big(\omega_{\mu\vec{k}}-\omega_{\nu\vec{k}_1}-\omega_{\eta\vec{k}_2}\big)t\big]\big[\hat{\bar{c}}^{\dagger}_{\mu\vec{k}}(t)+\hat{\bar{d}}^{\dagger}_{\mu\vec{k}}(t)\big]\hat{\bar{b}}_{\eta\vec{k}_2}(t).\tag{A20}$$

In principle, solving these differential equations with the initial conditions $\hat{\bar{d}}^{\dagger}_{\mu\vec{k}}(t_+)=\hat{d}^{\dagger}_{\mu\vec{k}}$, $\hat{\bar{c}}^{\dagger}_{\mu\vec{k}}(t_+)=\hat{c}^{\dagger}_{\mu\vec{k}}$, and $\hat{\bar{b}}^{\dagger}_{\mu\vec{k}}(t_+)=\hat{b}^{\dagger}_{\mu\vec{k}}$ allows us to compute $\hat{\bar{K}}_{a(b)}(t_-)$ defined by Eqs. (A12) and (A10) and then $|\psi_{\text{out}}\rangle$ by Eq. (A11). Indeed,

$$\hat{\bar{K}}_a(t_-)=\mathcal{A}\sum_{\mu}\int d\vec{k}\,f_p(\mu,\vec{k})\hat{\bar{c}}^{\dagger}_{\mu\vec{k}}(t_-),\quad \hat{\bar{K}}_b(t_-)=\mathcal{B}\sum_{\mu}\int d\vec{k}\,f_s(\mu,\vec{k})\hat{\bar{d}}^{\dagger}_{\mu\vec{k}}(t_-).\tag{A21}$$

Using assumption 3, as in Ref. [30] we solve the differential equations (A18) and (A19) at first order in V with time-dependent perturbation theory. We obtain

$$\hat{\bar{c}}^{\dagger}_{\mu\vec{k}}(t_-)\simeq\hat{c}^{\dagger}_{\mu\vec{k}}+\frac{1}{i}\sum_{\nu,\eta}\int d\vec{k}_1d\vec{k}_2S_{\nu\eta\mu}(\vec{k}_1,\vec{k}_2,\vec{k})\bigg[\int_{t_+}^{t_-}\exp\big[-i\big(\omega_{\mu\vec{k}}-\omega_{\nu\vec{k}_1}-\omega_{\eta\vec{k}_2}\big)t\big]dt\bigg]b^{\dagger}_{\nu\vec{k}_1}b^{\dagger}_{\eta\vec{k}_2},\tag{A22}$$

$$\begin{aligned}\hat{\bar{d}}^{\dagger}_{\eta\vec{k}}(t_-)\simeq&\hat{d}^{\dagger}_{\mu\vec{k}}+\frac{1}{i}\sum_{\nu,\eta,\mu'}\int d\vec{k}_1d\vec{k}_2d\vec{k}'f_{\mu,\eta}(\vec{k},\vec{k}_2)S^{*}_{\nu\eta\mu'}(\vec{k}_1,\vec{k}_2,\vec{k}')\bigg[\int_{t_+}^{t_-}\exp\big[i\big(\omega_{\mu'\vec{k}'}-\omega_{\nu\vec{k}_1}-\omega_{\eta\vec{k}_2}\big)t\big]dt\bigg]\hat{c}^{\dagger}_{\mu'\vec{k}'}\hat{b}_{\nu\vec{k}_1}\\&+\frac{1}{i}\sum_{\nu,\eta,\mu'}\int d\vec{k}_1d\vec{k}_2d\vec{k}'f_{\mu,\eta}(\vec{k},\vec{k}_2)S^{*}_{\nu\eta\mu'}(\vec{k}_1,\vec{k}_2,\vec{k}')\bigg[\int_{t_+}^{t_-}\exp\big[i\big(\omega_{\mu'\vec{k}'}-\omega_{\nu\vec{k}_1}-\omega_{\eta\vec{k}_2}\big)t\big]dt\bigg]\hat{d}^{\dagger}_{\mu'\vec{k}'}\hat{b}_{\nu\vec{k}_1}\\&+\frac{1}{i}\sum_{\nu,\eta}\int d\vec{k}_1d\vec{k}_2S_{\nu\eta\mu}(\vec{k}_1,\vec{k}_2,\vec{k})\bigg[\int_{t_+}^{t_-}\exp\big[-i\big(\omega_{\mu\vec{k}}-\omega_{\nu\vec{k}_1}-\omega_{\eta\vec{k}_2}\big)t\big]dt\bigg]\hat{b}^{\dagger}_{\nu\vec{k}_1}\hat{b}^{\dagger}_{\eta\vec{k}_2},\end{aligned}\tag{A23}$$

where all the operators appearing on the right-hand side of the equality are taken at time $t=t_+$. We note that the operator $\bar{d}^{+}_{\eta\vec{k}}(t_-)$ will be applied to the vacuum; therefore, the second and third terms of Eq. (A23) do not contribute.

The last term of Eq. (A23) will give a nonzero contribution only for frequencies $\omega_{\mu\vec{k}}$ in the range of the pump frequencies [this is a property of function $S_{\nu\eta\mu}(\vec{k}_1,\vec{k}_2,\vec{k})$]. However, at the end, the operator $\bar{d}^{\dagger}_{\eta\vec{k}}(t_-)$ will be used in the integral of Eq. (A21) defining $\bar{K}_b(t_-)$, where the effective range of integration is limited by the support of the function $f_s(\mu,k)$ defining the seed mode. Because of hypothesis 1 this range does not overlap with the one of the pump. The resulting integral is therefore zero. Therefore, we obtain that $\bar{d}^{\dagger}_{\eta\vec{k}}(t_-)=d^{\dagger}_{\mu\vec{k}}$ and

$$\hat{c}^{\dagger}_{\mu\vec{k}}(t_-)\simeq\hat{c}^{\dagger}_{\mu\vec{k}}+\frac{2\pi}{i}\sum_{\nu,\eta}\int d\vec{k}_1d\vec{k}_2S_{\nu\eta\mu}(\vec{k}_1,\vec{k}_2,\vec{k})\delta\big(\omega_{\mu\vec{k}}-\omega_{\nu\vec{k}_1}-\omega_{\eta\vec{k}_2}\big)\hat{b}^{\dagger}_{\nu\vec{k}_1}\hat{b}^{\dagger}_{\eta\vec{k}_2}.\tag{A24}$$

Finally, we obtain the expected result for $|\psi_{\text{out}}\rangle$,

$$|\psi_{\text{out}}\rangle = \exp\left(\mathcal{A}\sum_{\mu}\int d\vec{k}\, f_p(\mu,\vec{k})\hat{c}^{\dagger}_{\mu\vec{k}} - \text{H.c.}\right)|\text{vac}\rangle \otimes \exp\left[\left(\mathcal{A}\chi\sum_{\nu,\eta}\int d\vec{k}_1 d\vec{k}_2 L_{\nu,\eta}(\vec{k}_1,\vec{k}_2)\hat{b}^{\dagger}_{\nu\vec{k}_1}\hat{b}^{\dagger}_{\eta\vec{k}_2} - \text{H.c.}\right)\right]$$
$$\times \exp\left(\mathcal{B}\sum_{\mu}\int d\vec{k}\, f_s(\mu,\vec{k})\hat{d}^{\dagger}_{\mu\vec{k}} - \text{H.c.}\right)|\text{vac}\rangle, \tag{A25}$$

where we have defined the normalized function $L_{\nu,\eta}(\vec{k}_1,\vec{k}_2)$ as

$$L_{\nu,\eta}(\vec{k}_1,\vec{k}_2) = -\frac{2\pi i}{\chi}\sum_{\mu}\int d\vec{k}\, f_p(\mu,\vec{k})S_{\nu\eta\mu}(\vec{k}_1,\vec{k}_2,\vec{k})\delta\left(\omega_{\mu\vec{k}} - \omega_{\nu\vec{k}_1} - \omega_{\eta\vec{k}_2}\right), \tag{A26}$$

with χ a normalization factor defined as

$$\chi = 2\pi\left(\sum_{\nu,\eta}\int d\vec{k}_1 d\vec{k}_2\left|\sum_{\mu}\int d\vec{k}\, f_p(\mu,\vec{k})S_{\nu\eta\mu}(\vec{k}_1,\vec{k}_2,\vec{k})\delta(\omega_{\mu\vec{k}} - \omega_{\nu\vec{k}_1} - \omega_{\eta\vec{k}_2})\right|^2\right)^{1/2} \tag{A27}$$

such that

$$\sum_{\nu,\eta}\int d\vec{k}_1 d\vec{k}_2 |L_{\nu,\eta}(\vec{k}_1,\vec{k}_2)|^2 = 1.$$

Here $|\chi|^2$ is the probability of a photon pair generation per pump pulse photon in mode $f_p(\mu,\vec{k})$. Thus, $|\chi\mathcal{A}|^2$ is the total number of generated pairs of photons. We thus can identify the coefficient γ in main text [see also Eq. (A1)] to the product $\chi\mathcal{A}$. We stress that the validity of perturbation expansion [Eqs. (A22) and (A23)] is independent of the intensities $|\mathcal{A}|^2$ and $|\mathcal{B}|^2$ of the pump and the seed, respectively. It relies only on the smallness of $|\chi|^2$ (assumption 3).

APPENDIX B: SCHMIDT DECOMPOSITION

We provide here some useful information about the Schmidt mode decomposition. In order to perform a basis change to decompose Eq. (1) in the Schmidt basis we used that $\hat{S} = \gamma\iint L(\mathbf{k},\mathbf{k}')\hat{a}^{\dagger}_s(\mathbf{k})\hat{a}^{\dagger}_i(\mathbf{k}')d\mathbf{k}\,d\mathbf{k}' = \sum_n \sqrt{\lambda_n}\hat{b}^{\dagger}_n\hat{c}^{\dagger}_n$, where $\hat{b}^{\dagger}_n = \int \psi_n(\mathbf{k})\hat{a}^{\dagger}_s(\mathbf{k})d\mathbf{k}$ and $\hat{c}^{\dagger}_n = \int \phi_n(\mathbf{k})\hat{a}^{\dagger}_i(\mathbf{k})d\mathbf{k}$ are the Schmidt modes.

In addition, $L(\mathbf{k},\mathbf{k}') = \sum_n \sqrt{\lambda_n}\psi_n(\mathbf{k})\phi_n(\mathbf{k}')$. The ψ_n and ϕ_n form a basis in the spaces of the signal and the idler modes, respectively, with $\sqrt{\lambda_n} = \iint L(\mathbf{k},\mathbf{k}')\psi^*_n(\mathbf{k})\phi^*_n(\mathbf{k}')d\mathbf{k}\,d\mathbf{k}'$ and $\sqrt{\lambda_n}\psi_n(\mathbf{k}) = \int L(\mathbf{k},\mathbf{k}')\phi^*_n(\mathbf{k}')d\mathbf{k}'$ and analogously for $\phi_n(\mathbf{k})$. Using these relations, one can reproduce the results presented in Secs. II and III.

APPENDIX C: NOISE

We now discuss possible measurement imperfections. For this, we consider two independent sources of imperfections. The first one can be seen as noise in the $\mathbf{q}_i$ variables and may have different physical origins depending on the considered setup. For example, when measuring the spectral properties of photons, $\mathbf{q} \equiv t$, which is an optical path delay that is centered around some value, say, τ with a distribution $P(\tau + \delta\tau)$, where $\delta\tau$ is distributed around τ. The second one concerns the intrinsic discreteness of physical apparatuses, which means that the parameter $\mathbf{q}$ varies in finite steps and $\mathbf{q}_{i+1} = \mathbf{q}_i + \Delta\mathbf{q}$. Taking again as an example the case of spectral measurement, this would correspond to the minimum path difference between the interfering pulses.

We start by discussing the first case, which can be modeled as a random phase in the argument of, say, (21) as

$$\iiiint L(\mathbf{k},\mathbf{k}')e^{i\mathbf{k}(\mathbf{q}_\eta+\delta\mathbf{q}_\eta)}e^{i\mathbf{k}'(\mathbf{q}_\eta+\delta\mathbf{q}_\eta)}e^{i\mathbf{k}'(\mathbf{q}_\sigma+\delta\mathbf{q}_\sigma)}$$
$$\times P(\delta\mathbf{q}_\eta)P(\delta\mathbf{q}_\sigma)d\mathbf{k}\,d\mathbf{k}'d\delta\mathbf{q}_\sigma d\delta\mathbf{q}_\eta, \tag{C1}$$

where $P(\delta\mathbf{q}_\alpha)$ is a distribution. We can for instance consider it as a Gaussian function, with $P(\delta\mathbf{q}_\alpha) = \mathcal{N}e^{-\delta\mathbf{q}_\alpha{}^2/\Delta_\alpha}$. In this case, Eq. (C1) can be easily computed, leading to

$$\iint L(\mathbf{k},\mathbf{k}')e^{i\mathbf{k}\mathbf{q}_\eta}e^{i\mathbf{k}'\mathbf{q}_\eta}e^{i\mathbf{k}'\mathbf{q}_\sigma}e^{-(\mathbf{k}+\mathbf{k}')^2\Delta_\eta}e^{-\mathbf{k}'^2\Delta_\sigma}d\mathbf{k}\,d\mathbf{k}'. \tag{C2}$$

The expression above sets a relationship between the frequency range that can be detected and the precision of the measurement, since the widths Δ_η^{-1} and Δ_σ^{-1} are the cutoff frequencies, setting an effective width to the integral Eq. (C2). This is the usual condition observed in interferometric detection and can be met in different setups.

We now discuss the effect of a finite variation of $\mathbf{q}_\alpha$ variables. This leads to a sampling of $\tilde{L}(\mathbf{q},\mathbf{q}')$, in a number of (relevant) values that is proportional to the ratio between the width of the function $\tilde{L}(\mathbf{q},\mathbf{q}')$ and the intervals $\Delta\mathbf{q}$. A sampling rate of $1/\Delta\mathbf{q}$ ensures the reconstruction of $\tilde{L}(\mathbf{q},\mathbf{q}')$ from its Fourier coefficients through the Nyquist-Shannon sampling theorem.

With these relations in mind, it is possible to estimate the requirements a given experimental setup should meet to employ the presented method.

[1] C. Fabre and N. Treps, Modes and states in quantum optics, Rev. Mod. Phys. **92**, 035005 (2020).

[2] O. Morin, C. Fabre, and J. Laurat, Experimentally Accessing the Optimal Temporal Mode of Traveling Quantum Light States, Phys. Rev. Lett. **111**, 213602 (2013).

[3] A. Aspect, P. Grangier, and G. Roger, Experimental Realization of Einstein-Podolsky-Rosen-Bohm *Gedankenexperiment*: A New Violation of Bell's Inequalities, Phys. Rev. Lett. **49**, 91 (1982).

[4] S. Francesconi, F. Baboux, A. Raymond, N. Fabre, G. Boucher, A. Lemaître, P. Milman, M. I. Amanti, and S. Ducci, Engineering two-photon wavefunction and exchange statistics in a semiconductor chip, Optica **7**, 316 (2020).

[5] S. P. Walborn, A. N. de Oliveira, S. Pádua, and C. H. Monken, Multimode Hong-Ou-Mandel Interference, Phys. Rev. Lett. **90**, 143601 (2003).

[6] L. Sansoni, F. Sciarrino, G. Vallone, P. Mataloni, A. Crespi, R. Ramponi, and R. Osellame, Polarization Entangled State Measurement on a Chip, Phys. Rev. Lett. **105**, 200503 (2010).

[7] L. Lamata and J. Leon, Dealing with entanglement of continuous variables: Schmidt decomposition with discrete sets of orthogonal functions, J. Opt. B **7**, 224 (2005).

[8] J. M. Donohue, V. Ansari, J. Řeháček, Z. Hradil, B. Stoklasa, M. Paúr, L. L. Sánchez-Soto, and C. Silberhorn, Quantum-Limited Time-Frequency Estimation through Mode-Selective Photon Measurement, Phys. Rev. Lett. **121**, 090501 (2018).

[9] L. Vaidman, Teleportation of quantum states, Phys. Rev. A **49**, 1473 (1994).

[10] V. Ansari, B. Brecht, J. Gil-Lopez, J. M. Donohue, J. Řeháček, Z. Hradil, L. L. Sánchez-Soto, and C. Silberhorn, Achieving the ultimate quantum timing resolution, PRX Quantum **2**, 010301 (2021).

[11] J. Gil-Lopez, Y. S. Teo, S. De, B. Brecht, H. Jeong, C. Silberhorn, and L. L. Sánchez-Soto, Universal compressive tomography in the time-frequency domain, Optica **8**, 1296 (2021).

[12] C. Polycarpou, K. N. Cassemiro, G. Venturi, A. Zavatta, and M. Bellini, Adaptive Detection of Arbitrarily Shaped Ultrashort Quantum Light States, Phys. Rev. Lett. **109**, 053602 (2012).

[13] J. Roslund, R. M. de Araújo, S. Jiang, C. Fabre, and N. Treps, Wavelength-multiplexed quantum networks with ultrafast frequency combs, Nat. Photon. **8**, 109 (2014).

[14] N. Quesada and J. E. Sipe, Effects of time ordering in quantum nonlinear optics, Phys. Rev. A **90**, 063840 (2014).

[15] N. Quesada, G. Triginer, M. D. Vidrighin, and J. E. Sipe, Theory of high-gain twin-beam generation in waveguides: From Maxwell's equations to efficient simulation, Phys. Rev. A **102**, 033519 (2020).

[16] G. Triginer, M. D. Vidrighin, N. Quesada, A. Eckstein, M. Moore, W. S. Kolthammer, J. E. Sipe, and I. A. Walmsley, Understanding High-Gain Twin-Beam Sources Using Cascaded Stimulated Emission, Phys. Rev. X **10**, 031063 (2020).

[17] P. R. Sharapova, G. Frascella, M. Riabinin, A. M. Pérez, O. V. Tikhonova, S. Lemieux, R. W. Boyd, G. Leuchs, and M. V. Chekhova, Properties of bright squeezed vacuum at increasing brightness, Phys. Rev. Res. **2**, 013371 (2020).

[18] K. Zielnicki, K. Garay-Palmett, D. Cruz-Delgado, H. Cruz-Ramirez, M. F. O'Boyle, B. Fang, V. O. Lorenz, A. B. U'Ren, and P. G. Kwiat, Joint spectral characterization of photon-pair sources, J. Mod. Opt. **65**, 1141 (2018).

[19] M. Liscidini and J. E. Sipe, Stimulated Emission Tomography, Phys. Rev. Lett. **111**, 193602 (2013).

[20] L. A. Rozema, C. Wang, D. H. Mahler, A. Hayat, A. M. Steinberg, J. E. Sipe, and M. Liscidini, Characterizing an entangled-photon source with classical detectors and measurements, Optica **2**, 430 (2015).

[21] M. A. Ciampini, A. Geraldi, V. Cimini, C. Macchiavello, J. E. Sipe, M. Liscidini, and P. Mataloni, Stimulated emission tomography: Beyond polarization, Opt. Lett. **44**, 41 (2019).

[22] I. Jizan, B. Bell, L. G. Helt, A. C. Bedoya, C. Xiong, and B. J. Eggleton, Phase-sensitive tomography of the joint spectral amplitude of photon pair sources, Opt. Lett. **41**, 4803 (2016).

[23] M. Borghi, Phase-resolved joint spectra tomography of a ring resonator photon pair source using a silicon photonic chip, Opt. Express **28**, 7442 (2020).

[24] M. Lipka and M. Parniak, Single-Photon Hologram of a Zero-Area Pulse, Phys. Rev. Lett. **127**, 163601 (2021).

[25] F. A. Beduini, J. A. Zielińska, V. G. Lucivero, Y. A. de Icaza Astiz, and M. W. Mitchell, Interferometric Measurement of the Biphoton Wave Function, Phys. Rev. Lett. **113**, 183602 (2014).

[26] K.-K. Park, J.-H. Kim, T.-M. Zhao, Y.-W. Cho, and Y.-H. Kim, Measuring the frequency-time two-photon wavefunction of narrowband entangled photons from cold atoms via stimulated emission, Optica **4**, 1293 (2017).

[27] G. S. Thekkadath, B. A. Bell, R. B. Patel, M. S. Kim, and I. A. Walmsley, Measuring the Joint Spectral Mode of Photon Pairs Using Intensity Interferometry, Phys. Rev. Lett. **128**, 023601 (2022).

[28] F. A. Domínguez-Serna, A. B. U'Ren, and K. Garay-Palmett, Third-order parametric down-conversion: A stimulated approach, Phys. Rev. A **101**, 033813 (2020).

[29] P. Sharapova, A. M. Pérez, O. V. Tikhonova, and M. V. Chekhova, Schmidt modes in the angular spectrum of bright squeezed vacuum, Phys. Rev. A **91**, 043816 (2015).

[30] Z. Yang, M. Liscidini, and J. E. Sipe, Spontaneous parametric down-conversion in waveguides: A backward Heisenberg picture approach, Phys. Rev. A **77**, 033808 (2008).

[31] C. K. Law, I. A. Walmsley, and J. H. Eberly, Continuous Frequency Entanglement: Effective Finite Hilbert Space and Entropy Control, Phys. Rev. Lett. **84**, 5304 (2000).

[32] X. Chen, X. Li, and Z. Y. Ou, Direct temporal mode measurement of photon pairs by stimulated emission, Phys. Rev. A **101**, 033838 (2020).

[33] A. Jullien, U. Bortolozzo, S. Grabielle, J.-P. Huignard, N. Forget, and S. Residori, Continuously tunable femtosecond delay-line based on liquid crystal cells, Opt. Express **24**, 14483 (2016).

[34] S. Francesconi, A. Raymond, N. Fabre, A. Lemaître, M. I. Amanti, P. Milman, F. Baboux, and S. Ducci, Anyonic two-photon statistics with a semiconductor chip, ACS Photon. **8**, 2764 (2021).

[35] P. H. Souto Ribeiro, D. P. Caetano, M. P. Almeida, J. A. Huguenin, B. Coutinho dos Santos, and A. Z. Khoury, Observation of Image Transfer and Phase Conjugation in Stimulated Down-Conversion, Phys. Rev. Lett. **87**, 133602 (2001).

[36] P. H. Souto Ribeiro, S. Pádua, and C. H. Monken, Image and coherence transfer in the stimulated down-conversion process, Phys. Rev. A **60**, 5074 (1999).

[37] D. J. Kane and R. Trebino, Single-shot measurement of the intensity and phase of an arbitrary ultrashort pulse by using frequency-resolved optical gating, Opt. Lett. **18**, 823 (1993).

[38] V. Wong and I. A. Walmsley, Analysis of ultrashort pulse-shape measurement using linear interferometers, Opt. Lett. **19**, 287 (1994).

[39] S. Kurzyna, M. Jastrzębski, N. Fabre, W. Wasilewski, M. Lipka, and M. Parniak, Variable electro-optic shearing interferometry for ultrafast single-photon-level pulse characterization, Opt. Express **30**, 39826 (2022).

[40] Z. Yang, M. Jahanbozorgi, D. Jeong, S. Sun, O. Pfister, H. Lee, and X. Yi, A squeezed quantum microcomb on a chip, Nat. Commun. **12**, 4781 (2021).

[41] M. Pysher, Y. Miwa, R. Shahrokhshahi, R. Bloomer, and O. Pfister, Parallel Generation of Quadripartite Cluster Entanglement in the Optical Frequency Comb, Phys. Rev. Lett. **107**, 030505 (2011).

[42] J. F. Tasker, J. Frazer, G. Ferranti, E. Allen, L. Brunel, S. Tanzilli, V. D'Auria, and J. Matthews, Silicon photonics interfaced with integrated electronics for 9 GHz measurement of squeezed light, Nat. Photon. **15**, 11 (2021).

[43] S. Yokoyama, R. Ukai, S. C. Armstrong, C. Sornphiphatphong, T. Kaji, S. Suzuki, J.-i. Yoshikawa, H. Yonezawa, N. C. Menicucci, and A. Furusawa, Ultra-large-scale continuous-variable cluster states multiplexed in the time domain, Nat. Photon. **7**, 982 (2013).

[44] O. Pinel, J. Fade, D. Braun, P. Jian, N. Treps, and C. Fabre, Ultimate sensitivity of precision measurements with Gaussian quantum light: A multimodal approach, Phys. Rev. A **85**, 010101(R) (2012).

[45] O. Pinel, P. Jian, N. Treps, C. Fabre, and D. Braun, Quantum parameter estimation using general single-mode Gaussian states, Phys. Rev. A **88**, 040102(R) (2013).

[46] G. Maltese, M. I. Amanti, F. Appas, G. Sinnl, A. Lemaître, P. Milman, F. Baboux, and S. Ducci, Generation and symmetry control of quantum frequency combs, npj Quantum Inf. **6**, 13 (2020).

[47] B. Brecht, D. V. Reddy, C. Silberhorn, and M. G. Raymer, Photon Temporal Modes: A Complete Framework for Quantum Information Science, Phys. Rev. X **5**, 041017 (2015).

[48] N. Fabre, G. Maltese, F. Appas, S. Felicetti, A. Ketterer, A. Keller, T. Coudreau, F. Baboux, M. I. Amanti, S. Ducci, and P. Milman, Generation of a time-frequency grid state with integrated biphoton frequency combs, Phys. Rev. A **102**, 012607 (2020).

[49] N. Fabre, Quantum information in time-frequency continuous variables, Ph.D. thesis, Université de Paris, 2020.

[50] N. Fabre, A. Keller, and P. Milman, Time and frequency as quantum continuous variables, Phys. Rev. A **105**, 052429 (2022).

[51] Y. Chen, M. Fink, F. Steinlechner, J. P. Torres, and R. Ursin, Hong-Ou-Mandel interferometry on a biphoton beat note, npj Quantum Inf. **5**, 43 (2019).

[52] D. Branning, A. L. Migdall, and A. V. Sergienko, Simultaneous measurement of group and phase delay between two photons, Phys. Rev. A **62**, 063808 (2000).

[53] M. Liscidini, L. G. Helt, and J. E. Sipe, Asymptotic fields for a Hamiltonian treatment of nonlinear electromagnetic phenomena, Phys. Rev. A **85**, 013833 (2012).